



Contents lists available at SciVerse ScienceDirect

# Spectrochimica Acta Part A: Molecular and Biomolecular Spectroscopy

journal homepage: [www.elsevier.com/locate/saa](http://www.elsevier.com/locate/saa)

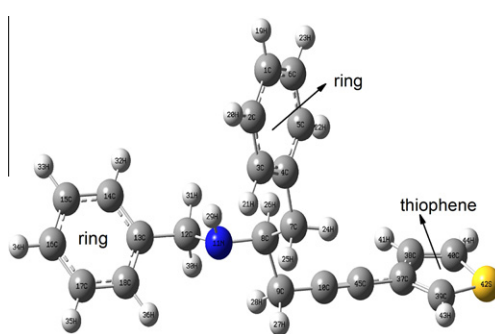
## Synthesis, analysis of spectroscopic and nonlinear optical properties of the novel compound: (*S*)-*N*-benzyl-1-phenyl-5-(thiophen-3-yl)-4-pentyn-2-amine

Mehmet Karabacak<sup>a,\*</sup>, Caglar Karaca<sup>b</sup>, Ahmet Atac<sup>b</sup>, Mustafa Eskici<sup>c</sup>, Abdullah Karanfil<sup>c</sup>, Etem Kose<sup>b</sup><sup>a</sup> Department of Physics, Afyon Kocatepe University, Afyonkarahisar, Turkey<sup>b</sup> Department of Physics, Celal Bayar University, Manisa, Turkey<sup>c</sup> Department of Chemistry, Celal Bayar University, Manisa, Turkey

### HIGHLIGHTS

- ▶ Spectroscopic properties of the novel molecule were examined by FT-IR, NMR and UV techniques and DFT.
- ▶ The complete assignments were performed on the basis of the total energy distribution (TED).
- ▶ Nonlinear optical properties of the molecule were studied.
- ▶ HOMO and LUMO energies, molecular electrostatic potential distribution of the molecule were calculated.

### GRAPHICAL ABSTRACT



### ARTICLE INFO

#### Article history:

Received 22 March 2012

Received in revised form 10 May 2012

Accepted 20 May 2012

Available online 7 July 2012

#### Keywords:

(*S*)-*N*-benzyl-1-phenyl-5-(thiophen-3-yl)-4-pentyn-2-amineFT-IR, <sup>13</sup>C, <sup>1</sup>H NMR and UV spectra

DFT

HOMO–LUMO

Nonlinear optical properties

### ABSTRACT

In this study, a novel compound (*S*)-*N*-benzyl-1-phenyl-5-(thiophen-3-yl)-4-pentyn-2-amine (abbreviated as BPTPA) was synthesized and structurally characterized by FT-IR, NMR and UV spectroscopy. The molecular geometry and vibrational frequencies of BPTPA in the ground state have been calculated by using the density functional method (B3LYP) invoking 6-311++G(d,p) basis set. The geometry of the molecule was fully optimized, vibrational spectra were calculated. The fundamental vibrations were assigned on the basis of the total energy distribution (TED) of the vibrational modes, calculated with scaled quantum mechanics (SQM) method and PQS program. Total and partial density of state (TDOS and PDOS) and also overlap population density of state (OPDOS) diagrams analysis were given. The energy and oscillator strength of each excitation were calculated by time-dependent density functional theory (TD-DFT) results complements with the experimental findings. The NMR chemical shifts (<sup>1</sup>H and <sup>13</sup>C) were recorded and calculated using the gauge invariant atomic orbital (GIAO) method. The dipole moment, linear polarizability and first hyperpolarizability values were also computed. The linear polarizability and first hyper polarizability of the studied molecule indicate that the compound is a good candidate of nonlinear optical materials. Finally, vibrational wavenumbers, absorption wavelengths and chemical shifts were compared with calculated values, and found to be in good agreement with experimental results.

© 2012 Elsevier B.V. All rights reserved.

### Introduction

Thiophene-containing compounds are known as materials with potential applications in the flavor [1] and pharmaceutical indus-

tries [2], in conducting polymer design [3], as well as in nonlinear optical materials [4]. Thiophene derivatives are also often used as intermediates in a wide range of areas of synthetic chemistry. The insertion of thiophene in the linear ethynyl–phenyl conjugated chain, gives a higher electron delocalization to the molecule [5]. In general, the conjugated molecules, integrating the thiophene rings and the end-capped *N,N*-dimethyl-amino-phenyl moiety, of

\* Corresponding author. Tel.: +90 272 2281311; fax: +90 272 2281235.

E-mail address: [karabacak@aku.edu.tr](mailto:karabacak@aku.edu.tr) (M. Karabacak).

precise length and constitution, exhibit high thermal stability [6,7] and show intrinsic electronic properties such as: luminescence [8], redox [9] and charge transport [10].

The structure of thiophene was thoroughly studied theoretically, as well as, experimentally in gas phase, liquid and solid phase [11–16]. It was studied in 1965 by Rico et al. [17] and the assignments of fundamental modes were proposed. Klots et al. [14] made a detailed vibrational analysis of thiophene in vapor phase and obtained a complete set of vibrational wavenumbers of the fundamental modes. Vibrational analysis of thiophene and its solvation in two polar solvents (DMSO and methanol) by Raman spectroscopy combined with *ab initio* and DFT calculations were studied by Singh et al. [15].

DFT has emerged as a powerful tool in studying vibrational spectra of fairly large molecules. The DFT calculations are reported to provide excellent vibrational frequencies of organic compounds if the calculated frequencies are scaled to compensate for the approximate treatment of electron correlation, for basis set deficiencies and for the anharmonicity [16–19]. GIAO/DFT approach is widely used for the calculations of chemical shifts for a variety of heterocyclic compounds [20–22]. Therefore, we have utilized the gradient corrected DFT [23] with the Becke's three-parameter hybrid functional (B3) [24] for the exchange part and the Lee–Yang–Parr (LYP) correlation function [25], accepted as a cost-effective approach, for the computation of molecular structure, vibrational frequencies and energies of optimized structures.

As a part of the research aimed at investigation of the reactivity of cyclic sulfamidates towards acetylides, (*S*)-*N*-benzyl-1-phenyl-5-(thiophen-3-yl)-4-pentyn-2-amine is synthesized using the reaction of phenylalanine-derived 1,2-cyclic sulfamidate with the acetylide prepared from 3-ethynylthiophene [26] and structurally characterized FT-IR, NMR and UV spectroscopy. A comprehensive theoretical structurally characterization of the title compound including FT-IR, NMR and UV calculations by using the density functional method (B3LYP) invoking 6-311++G(d,p) basis set is presented in this study. The results of theoretical characterization were compared with experimental characterization data. Besides these, the dipole moment, nonlinear optical (NLO) properties, linear polarizability and first hyperpolarizability, chemical hardness and Mulliken atomic charge were also studied using the same method and basis set. As a result, vibrational wavenumbers, absorption wavelengths and chemical shifts values are in fairly good agreement with the experimental results.

## Experimental

### Materials

Hexamethylphosphoramide (HMPA) was distilled from sodium metal and tetrahydrofuran (THF) was freshly distilled from LiAlH<sub>4</sub>

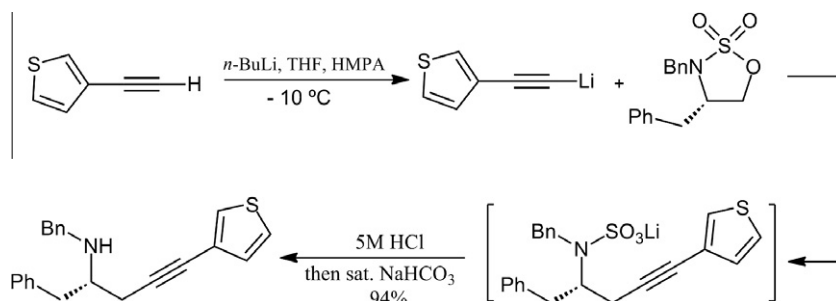
before use. 3-Ethynylthiophene (96%) was purchased from Aldrich Chemical Company (USA) and used as received. (*S*)-3,4-dibenzyl-1,2,3-oxathiazolidine-2,2-dioxide was prepared according to the literature procedure [27].

### Synthesis of *N*-benzyl-1-phenyl-5-(thiophen-3-yl)-4-pentyn-2-amine

To a stirred solution of 3-ethynylthiophene (503 mg, 4.46 mmol) in 15 mL freshly distilled dry THF containing 1.5 mL HMPA cooled at  $-10\text{ }^{\circ}\text{C}$  (ice-salt) under argon atmosphere was added drop wise *n*-butyl lithium (2.9 mL, 4.62 mmol, 15% solution in *n*-hexane). After stirring at  $-10\text{ }^{\circ}\text{C}$  for 1 h, a solution of (4*S*)-3,4-dibenzyl [1–3]oxathiazolidine-2,2-dioxide (705 mg, 2.32 mmol) in 3 mL dry THF was added to the resulting acetylide solution via a syringe and stirring continued for additional 2 h. The reaction mixture was allowed to warm up to room temperature and then treated with 5 M 3 mL HCl solution to hydrolyze the *N*-sulfate intermediate for 2 h before neutralization with saturated NaHCO<sub>3</sub> solution. Extraction with ether three times and drying over anhydrous Na<sub>2</sub>SO<sub>4</sub> followed by evaporation of volatiles *in vacuo* gave the crude product. Purification by column chromatography using a (EtOAc: hexane (1:10) to (1:6) gradient) solvent system containing 0.5% triethylamine afforded (*S*)-*N*-benzyl-1-phenyl-5-(2-thiophen-3-yl)-pent-4-yn-2-amine as a pale yellow oil (720 mg, 94% yield). Partial decomposition of the product on silica was also observed. Rf: 0.59 [(EtOAc:Hexane) 1:3]; [ $\alpha$ ]<sub>D</sub><sup>20</sup> + 8.4 (*c* = 1, CHCl<sub>3</sub>); IR (film);  $\nu_{\text{max}}/\text{cm}^{-1}$  3328 (NH), 2228 (C≡C), 1602, 1584, 1520, 1462 (aromatic C≡C),  $\delta_{\text{H}}$  (400, MHz, CDCl<sub>3</sub>) (ppm) 2.48 (1H, dd, *J* = 5.6 and 17), 2.54 (1H, dd, *J* = 5.6 and 17), 2.85–2.93 (2H, m), 3.04 (1H, quintet, *J* = 5.6), 3.81 (1H, d, *J* = 13.2), 3.89 (1H, d, *J* = 13.2), 7.08 (1H, dd, *J* = 1.2 and 4.8, Ar–H), 7.19–7.30 (11H, m, Ar–H), 7.35 (1H, dd, *J* = 0.8 and 2.8, Ar–H);  $\delta_{\text{C}}$  (100 MHz, CDCl<sub>3</sub>) (ppm) 24.39, 40.78, 51.42, 57.52, 78.23, 86.92, 122.96, 125.34, 126.58, 127.16, 128.17, 128.29, 128.64, 128.70, 129.65, 130.27, 139.19, 140.62; HRMS (CI): [M+H]<sup>+</sup> found 332.1472, C<sub>22</sub>H<sub>21</sub>NS requires 332.1473 (Scheme 1).

### FT-IR, NMR and UV measurements

The FT-IR spectrum of BPTPA was recorded in the region 600–4000 cm<sup>-1</sup> on a Perkin-Elmer FT-IR System Spectrum BX spectrometer which was calibrated using polystyrene bands. The ultraviolet absorption spectrum of BPTPA, solved in water, ethanol and chloroform, was examined in the range 200–400 nm using Shimadzu UV-1700 PC, UV-vis recording Spectrophotometer. NMR chemical shifts were recorded in Varian Infinity Plus spectrometer at 300 K. The compound was dissolved in chloroform. Chemical shifts were reported in ppm relative to tetramethylsilane (TMS) for <sup>1</sup>H and <sup>13</sup>C NMR spectra. The <sup>1</sup>H, <sup>13</sup>C and APT NMR spectra were used for the full characterization of the compound.



Scheme 1. Synthesis of (*S*)-*N*-benzyl-1-phenyl-5-(thiophen-3-yl)-4-pentyn-2-amine.

## Computational details

The computational work aim to determine the optimize geometry of the novel compound. The entire calculations were performed at DFT/B3LYP [24,25] with the 6-311++G(d,p) basis set levels on a personal computer using Gaussian 09 [28] program package, invoking gradient geometry optimization [29]. Optimized structural parameters, vibrational frequency, isotropic chemical shift, electronic and nonlinear optical properties were calculated. The vibrational frequencies were calculated with this method, and wavenumbers in the ranges from 4000 to 1700  $\text{cm}^{-1}$  and lower than 1700  $\text{cm}^{-1}$  were scaled with 0.958 and 0.983, respectively, in order to improve the agreement with the experimental results [30]. The theoretical results have enabled us to make the detailed assignments of the experimental FT-IR spectra of the title molecule. The TED was calculated by using the SQM method and PQS program [31]. The fundamental vibrational modes were characterized by their TED. The  $^1\text{H}$  and  $^{13}\text{C}$  NMR chemical shifts ( $\delta_{\text{H}}$  and  $\delta_{\text{C}}$ ) of the compound were calculated using the GIAO method [32] in chloroform. The electronic properties were also calculated using B3LYP method of the time-dependent DFT (TD-DFT) [33–35], basing on the optimized structure. TD-DFT has been proved to be a powerful and effective computational tool for the study of the ground and excited state properties by comparison to the available experimental data. Hence, we used TD-DFT to obtain wavelengths and compared the calculated results with the experimental UV absorption values. Moreover, the dipole moment, nonlinear optical (NLO) properties, linear polarizabilities and first hyperpolarizabilities, chemical hardness and Mulliken atomic charge were also been studied using B3LYP/6-311++G(d,p).

## Results and discussion

### Molecular geometry

The optimized geometrical parameters of BPTPA, calculated by DFT/B3LYP/6-311++G(d,p) were listed in Table 1, in accordance with numbering scheme given in Fig. 1. In the present study, we employed full geometry optimization for BPTPA without symmetry constraint. The optimized structure can only be compared with other similar systems for which the crystal structures have been solved [36–38]. The geometry of the molecule are determined belong to a true minimum proven by all real wavenumbers in the vibrational analysis as seen from the Table 2. The optimized bond lengths of C–C in the phenyl ring fall in the range from 1.392 to 1.402 Å for B3LYP/6-311++G(d,p) which are in good agreement with those of structurally similar systems whose crystal structures are elucidated (1.371–1.402 Å) [36–38]. The optimized C–N bond lengths were calculated between 1.464 and 1.467 Å, show good coherent with the observed as 1.46 Å for a similar structure [36]. These values showed more consistency with our calculation results. The bond length  $\text{S}_{42}\text{--C}_{39}$  was predicted at 1.726 Å (DFT), observed as 1.727 Å [36]. However, particularly the X–H bond lengths are predicted systematically too long from DFT method [39,40]. This theoretical pattern also is found for BPTPA, since the large deviation from experimental X–H bond lengths may arise from the low scattering of hydrogen atoms in the X-ray diffraction experiment.

The bond angles of BPTPA were given in Table 1 are good agreement with similar structures. For example, the bond angles of the C–C–C of the phenyl rings were observed between 117° and 123° [36–38] and calculated 119.5–121.0°. The calculated bond angles are better than experimental results according to the expected normal values 120°. Based on above comparison, although there are some differences between the theoretical and experimental values, the optimized structural parameters can well reproduce the experimental one.

**Table 1**

The optimized geometry (bond lengths (Å) and bond angles (°)) of BPTPA.

Bond lengths	X-ray <sup>a,b,c</sup>	B3LYP	Bond angles	X-ray <sup>a,b,c</sup>	B3LYP
C <sub>1</sub> –C <sub>2</sub>	1.39 <sup>a</sup>	1.393	C <sub>2</sub> –C <sub>1</sub> –C <sub>6</sub>	117 <sup>a</sup>	119.5
C <sub>1</sub> –C <sub>6</sub>	1.40 <sup>a</sup>	1.395	C <sub>2</sub> –C <sub>1</sub> –H <sub>19</sub>		120.3
C <sub>1</sub> –H <sub>19</sub>		1.084	C <sub>6</sub> –C <sub>1</sub> –H <sub>19</sub>		120.2
C <sub>2</sub> –C <sub>3</sub>	1.40 <sup>a</sup>	1.396	C <sub>1</sub> –C <sub>2</sub> –C <sub>3</sub>	120 <sup>a</sup>	120.1
C <sub>2</sub> –H <sub>20</sub>		1.085	C <sub>1</sub> –C <sub>2</sub> –H <sub>20</sub>		120.1
C <sub>3</sub> –C <sub>4</sub>	1.40 <sup>a</sup>	1.400	C <sub>3</sub> –C <sub>2</sub> –H <sub>20</sub>		119.8
C <sub>3</sub> –H <sub>21</sub>		1.086	C <sub>2</sub> –C <sub>3</sub> –C <sub>4</sub>	123 <sup>a</sup>	121.0
C <sub>4</sub> –C <sub>5</sub>	1.41 <sup>a</sup>	1.402	C <sub>2</sub> –C <sub>3</sub> –H <sub>21</sub>		119.6
C <sub>4</sub> –C <sub>7</sub>	1.50 <sup>a</sup>	1.513	C <sub>4</sub> –C <sub>3</sub> –H <sub>21</sub>		119.4
C <sub>5</sub> –C <sub>6</sub>	1.4 <sup>a</sup>	1.392	C <sub>3</sub> –C <sub>4</sub> –C <sub>5</sub>	117 <sup>a</sup>	118.2
C <sub>5</sub> –H <sub>22</sub>		1.086	C <sub>3</sub> –C <sub>4</sub> –C <sub>7</sub>	124 <sup>a</sup>	121.4
C <sub>6</sub> –H <sub>23</sub>		1.085	C <sub>5</sub> –C <sub>4</sub> –C <sub>7</sub>	118 <sup>a</sup>	120.4
C <sub>7</sub> –C <sub>8</sub>	1.54 <sup>a</sup>	1.542	C <sub>4</sub> –C <sub>5</sub> –C <sub>6</sub>	120 <sup>a</sup>	120.9
C <sub>7</sub> –H <sub>24</sub>		1.093	C <sub>4</sub> –C <sub>5</sub> –H <sub>22</sub>		119.4
C <sub>7</sub> –H <sub>25</sub>		1.095	C <sub>6</sub> –C <sub>5</sub> –H <sub>22</sub>		119.6
C <sub>8</sub> –C <sub>9</sub>	1.54 <sup>a</sup>	1.551	C <sub>1</sub> –C <sub>6</sub> –C <sub>5</sub>	122 <sup>a</sup>	120.2
C <sub>8</sub> –N <sub>11</sub>	1.46 <sup>a</sup>	1.464	C <sub>1</sub> –C <sub>6</sub> –H <sub>23</sub>		120.0
C <sub>8</sub> –H <sub>26</sub>		1.103	C <sub>5</sub> –C <sub>6</sub> –H <sub>23</sub>		119.8
C <sub>9</sub> –C <sub>10</sub>		1.459	C <sub>4</sub> –C <sub>7</sub> –C <sub>8</sub>	110 <sup>a</sup>	113.9
C <sub>9</sub> –H <sub>27</sub>		1.096	C <sub>4</sub> –C <sub>7</sub> –H <sub>24</sub>		109.6
C <sub>9</sub> –H <sub>28</sub>		1.095	C <sub>4</sub> –C <sub>7</sub> –H <sub>25</sub>		109.9
C <sub>10</sub> –C <sub>45</sub>	1.202 <sup>c</sup>	1.206	C <sub>8</sub> –C <sub>7</sub> –H <sub>24</sub>		107.8
N <sub>11</sub> –C <sub>12</sub>	1.461 <sup>b</sup>	1.467	C <sub>8</sub> –C <sub>7</sub> –H <sub>25</sub>		108.2
N <sub>11</sub> –H <sub>29</sub>		1.016	H <sub>24</sub> –C <sub>7</sub> –H <sub>25</sub>		107.2
C <sub>12</sub> –C <sub>13</sub>	1.454 <sup>b</sup>	1.514	C <sub>7</sub> –C <sub>8</sub> –C <sub>9</sub>	110 <sup>a</sup>	110.4
C <sub>12</sub> –H <sub>30</sub>		1.096	C <sub>7</sub> –C <sub>8</sub> –N <sub>11</sub>	118 <sup>a</sup>	109.9
C <sub>12</sub> –H <sub>31</sub>		1.103	C <sub>7</sub> –C <sub>8</sub> –H <sub>26</sub>		108.1
C <sub>13</sub> –C <sub>14</sub>	1.377 <sup>b</sup>	1.397	C <sub>9</sub> –C <sub>8</sub> –N <sub>11</sub>	110 <sup>a</sup>	109.6
C <sub>13</sub> –C <sub>18</sub>	1.398 <sup>b</sup>	1.400	C <sub>9</sub> –C <sub>8</sub> –H <sub>26</sub>		107.6
C <sub>14</sub> –C <sub>15</sub>	1.358 <sup>b</sup>	1.396	N <sub>11</sub> –C <sub>8</sub> –H <sub>26</sub>		111.2
C <sub>14</sub> –H <sub>32</sub>		1.086	C <sub>8</sub> –C <sub>9</sub> –C <sub>10</sub>		113.7
C <sub>15</sub> –C <sub>16</sub>	1.394 <sup>b</sup>	1.392	C <sub>8</sub> –C <sub>9</sub> –H <sub>27</sub>		108.4
C <sub>15</sub> –H <sub>33</sub>		1.085	C <sub>8</sub> –C <sub>9</sub> –H <sub>28</sub>		109.2
C <sub>16</sub> –C <sub>17</sub>	1.371 <sup>b</sup>	1.396	C <sub>10</sub> –C <sub>9</sub> –H <sub>27</sub>		110.2
C <sub>16</sub> –H <sub>34</sub>		1.084	C <sub>10</sub> –C <sub>9</sub> –H <sub>28</sub>		108.8
C <sub>17</sub> –C <sub>18</sub>	1.398 <sup>b</sup>	1.392	H <sub>27</sub> –C <sub>9</sub> –H <sub>28</sub>		106.2
C <sub>17</sub> –H <sub>35</sub>		1.085	C <sub>8</sub> –N <sub>11</sub> –C <sub>12</sub>	115 <sup>a</sup>	115.1
C <sub>18</sub> –H <sub>36</sub>		1.084	C <sub>8</sub> –N <sub>11</sub> –H <sub>29</sub>		109.3
C <sub>37</sub> –C <sub>38</sub>	1.421 <sup>c</sup>	1.439	C <sub>12</sub> –N <sub>11</sub> –H <sub>29</sub>		108.3
C <sub>37</sub> –C <sub>39</sub>	1.377 <sup>c</sup>	1.377	N <sub>11</sub> –C <sub>12</sub> –C <sub>13</sub>	110 <sup>a</sup>	111.6
C <sub>37</sub> –C <sub>45</sub>	1.422 <sup>c</sup>	1.422	N <sub>11</sub> –C <sub>12</sub> –H <sub>30</sub>		108.4
C <sub>38</sub> –C <sub>40</sub>	1.377 <sup>c</sup>	1.362	N <sub>11</sub> –C <sub>12</sub> –H <sub>31</sub>		112.2
C <sub>38</sub> –H <sub>41</sub>		1.081	C <sub>13</sub> –C <sub>12</sub> –H <sub>30</sub>		108.9
C <sub>39</sub> –S <sub>42</sub>	1.727 <sup>c</sup>	1.726	C <sub>13</sub> –C <sub>12</sub> –H <sub>31</sub>		109.2
C <sub>39</sub> –H <sub>43</sub>		1.079	H <sub>30</sub> –C <sub>12</sub> –H <sub>31</sub>		106.3
C <sub>40</sub> –S <sub>42</sub>	1.730 <sup>c</sup>	1.735	C <sub>12</sub> –C <sub>13</sub> –C <sub>14</sub>		120.7
C <sub>40</sub> –H <sub>44</sub>		1.079	C <sub>12</sub> –C <sub>13</sub> –C <sub>18</sub>		120.6
C <sub>13</sub> –C <sub>18</sub> –C <sub>17</sub>	120 <sup>b</sup>	120.64	C <sub>14</sub> –C <sub>13</sub> –C <sub>18</sub>		118.6
C <sub>13</sub> –C <sub>18</sub> –H <sub>36</sub>		119.12	C <sub>13</sub> –C <sub>14</sub> –C <sub>15</sub>	121.3 <sup>b</sup>	120.8
C <sub>17</sub> –C <sub>18</sub> –H <sub>36</sub>		120.24	C <sub>13</sub> –C <sub>14</sub> –H <sub>32</sub>		119.5
C <sub>38</sub> –C <sub>37</sub> –C <sub>39</sub>	111.7 <sup>c</sup>	111.7	C <sub>15</sub> –C <sub>14</sub> –H <sub>32</sub>		119.7
C <sub>38</sub> –C <sub>37</sub> –C <sub>45</sub>	121.95 <sup>c</sup>	124.0	C <sub>14</sub> –C <sub>15</sub> –C <sub>16</sub>	120.1 <sup>b</sup>	120.0
C <sub>39</sub> –C <sub>37</sub> –C <sub>45</sub>	126.8 <sup>c</sup>	124.3	C <sub>14</sub> –C <sub>15</sub> –H <sub>33</sub>		119.8
C <sub>37</sub> –C <sub>38</sub> –C <sub>40</sub>	113.1 <sup>c</sup>	113.0	C <sub>16</sub> –C <sub>15</sub> –H <sub>33</sub>		120.1
C <sub>37</sub> –C <sub>38</sub> –H <sub>41</sub>		123.0	C <sub>15</sub> –C <sub>16</sub> –C <sub>17</sub>	121 <sup>b</sup>	119.6
C <sub>40</sub> –C <sub>38</sub> –H <sub>41</sub>		124.0	C <sub>15</sub> –C <sub>16</sub> –H <sub>34</sub>		120.2
C <sub>37</sub> –C <sub>39</sub> –S <sub>42</sub>	111.7 <sup>c</sup>	112.1	C <sub>17</sub> –C <sub>16</sub> –H <sub>34</sub>		120.2
C <sub>37</sub> –C <sub>39</sub> –H <sub>43</sub>		127.5	C <sub>16</sub> –C <sub>17</sub> –C <sub>18</sub>		120.2
S <sub>42</sub> –C <sub>39</sub> –H <sub>43</sub>		120.5	C <sub>16</sub> –C <sub>17</sub> –H <sub>35</sub>		120.0
C <sub>38</sub> –C <sub>40</sub> –S <sub>42</sub>	111.2 <sup>c</sup>	111.7	C <sub>18</sub> –C <sub>17</sub> –H <sub>35</sub>		119.8
C <sub>38</sub> –C <sub>40</sub> –H <sub>44</sub>		128.4			
S <sub>42</sub> –C <sub>40</sub> –H <sub>44</sub>		119.9			
C <sub>39</sub> –S <sub>42</sub> –C <sub>40</sub>	91.8 <sup>c</sup>	91.6			

<sup>a</sup> Ref. [36].

<sup>b</sup> Ref. [37].

<sup>c</sup> Ref. [38].

### Vibrational analysis

The vibrational frequencies were obtained using DFT/B3LYP methods using split valence basis sets along with diffuse and polarization function with 6-311++G(d,p) basis set. The selected calcu-

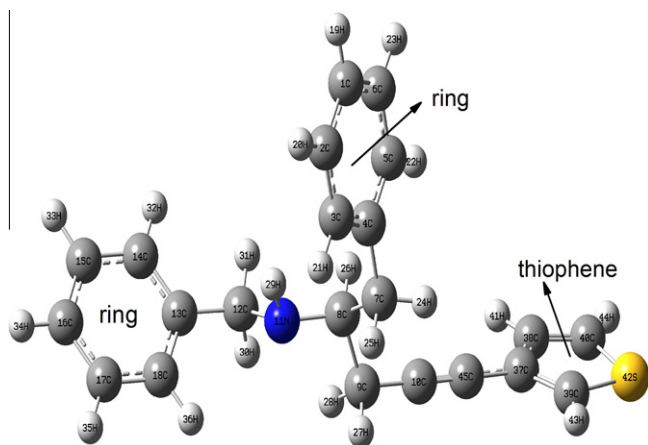


**Fig. 1.** The theoretical optimized geometric structure and atoms numbering of BPTPA.

lated wavenumbers are given in Table 2. The experimental frequencies given in the same table, is based on the FT-IR spectra of BPTPA shown Fig. 2. The all calculated wavenumbers are given in Supplementary material (Table S1). The vibrational analysis of BPTPA is performed on the basis of the characteristic vibration modes of C≡C, C–C, NH, CH and CH<sub>2</sub> groups of the compound.

The title molecule is non-planar and belongs to C<sub>1</sub> point group symmetry has no relevant distribution of species.

It is stated that the N–H stretching vibrations occur in the region 3300–3500 cm<sup>-1</sup> [41]. In this study, we predicted 3363 cm<sup>-1</sup> (ν129), assigned to N–H stretching vibration, recorded at 3328 cm<sup>-1</sup> in the FT-IR spectrum. This mode is a pure mode as is evident from TED column contributing exactly 100%.

The C–N stretching mode is a rather difficult task since there are problems in identifying these frequencies from other vibrations. Silverstein [42] assigned C–N stretching absorption in the region 1386–1266 cm<sup>-1</sup> for aromatic amines. This mode is observed at 1293 cm<sup>-1</sup> by Bellamy et al. [43]. In this study, the C–N stretching vibration is observed at 1180 cm<sup>-1</sup> and the computed values are predicted at 1105 and 1115 cm<sup>-1</sup> (modes ν71 and ν72). There is a discrepancy which, may be due to mixing with C–C vibration. One can see TED value contributing to 25% and 77% as shown Table 2.

The hetero-aromatic structure shows the presence of C–H stretching vibration in the region 3100–3000 cm<sup>-1</sup>, which is the characteristic region for the ready identification of C–H stretching vibration [42,44,45]. The C–H stretching vibrations were calculated at 3021–3055 cm<sup>-1</sup> showed very good coherent with the experimental data. For example the experimental value is assigned at 3026 cm<sup>-1</sup>, the calculated one is obtained at 3021 cm<sup>-1</sup>. These modes are pure stretching modes as seen from the TED column shown in Table 2. The in-plane C–H bending vibrations appear in

**Table 2**

Comparison of the selected calculated harmonic frequencies and experimental (FT-IR) wavenumbers (cm<sup>-1</sup>) using by B3LYP methods 6-311++G(d,p) of BPTPA.

Modes No.	Exp. FT-IR	Theoretical			TED <sup>b</sup> (≥10%)
		Unscaled freq.	Scaled freq. <sup>a</sup>	<i>f</i> <sub>Infrared</sub>	
V <sub>34</sub>	626	636	626	0.53	δCCC(58) ring + δCCH(20) ring
V <sub>38</sub>	696	710	698	32.19	τCCCH(49)ring + τCCCC(38)ring
V <sub>41</sub>	746	758	745	37.51	τCCCH(39)ring + τCCCC(14)ring
V <sub>43</sub>	780	785	772	37.04	γCH(89) thio
V <sub>50</sub>	858	862	848	1.82	vCC(36)
V <sub>53</sub>	894	907	892	6.10	δCCC(21)thio + δCCS(14)thio + δSCH(12)thio + vC10C9(12)
V <sub>54</sub>	910	924	909	0.78	γCH(76) ring
V <sub>55</sub>	928	945	929	0.86	γCH(74) ring
V <sub>58</sub>	976	991	974	3.13	rCH <sub>2</sub> (29) + τCHCH(15) ring
V <sub>62</sub>	1004	1017	1000	0.57	vCC(37) ring + δCCC(37) ring {trigonal ring breathing}
V <sub>64</sub>	1014	1031	1014	12.10	vCC(33) + vCC(17) thio
V <sub>65</sub>	1028	1047	1029	5.17	vCC(25) ring + δCCH(15) ring + vC8C7(14)
V <sub>68</sub>	1078	1095	1077	3.99	vCC(25) ring + δCCH(18) ring
V <sub>72</sub>	1118	1135	1115	49.41	vCN(77)
V <sub>76</sub>	1180	1200	1179	1.54	vCC(17) ring + δCCH(76) ring
V <sub>79</sub>	1202	1223	1202	1.05	vC12–C <sub>ring</sub> (39) + vCC(19) ring + δCCH(10) ring
V <sub>81</sub>	1218	1246	1225	11.94	tCH <sub>2</sub> (46)
V <sub>82</sub>	1232	1253	1232	0.10	tCH <sub>2</sub> (40)
V <sub>84</sub>	1278	1306	1284	13.47	ωCH <sub>2</sub> (50) + δCCH(11)
V <sub>85</sub>	1300	1329	1306	0.39	ωCH <sub>2</sub> (52) + δCCH(10)
V <sub>91</sub>	1358	1378	1354	21.83	ωCH <sub>2</sub> (22) + δ CH <sub>2</sub> (18) + v CC(10) thio.
V <sub>94</sub>	1428	1451	1426	7.83	vCC(80) thio + δCCH (10) thio
V <sub>95</sub>	1454	1470	1445	11.2	ρCH <sub>2</sub> (94)
V <sub>97</sub>	1462	1482	1457	6.06	δCCH(46) ring + vCC(28) ring
V <sub>98</sub>	1470	1489	1464	8.24	ρCH <sub>2</sub> (69)
V <sub>100</sub>	1493	1513	1487	57.91	ρCH <sub>2</sub> (53) + δ CNH(34)
V <sub>103</sub>	1520	1563	1537	3.89	vC = C <sub>thio</sub> (57) + δ CCH(14) thio. + v C <sub>37</sub> C <sub>45</sub> (10) + δCCC(10) thio.
V <sub>104</sub>	1584	1622	1594	0.84	vCC(69) ring + δCCH(12) ring
V <sub>105</sub>	1602	1623	1596	0.84	vCC(70) ring + δCCH(12) ring
V <sub>108</sub>	2228	2326	2228	2.68	vC≡C(100)
V <sub>111</sub>	2847	3025	2898	23.46	v <sub>sym</sub> CH <sub>2</sub> (97)
V <sub>114</sub>	2920	3060	2932	15.26	v <sub>asym</sub> CH <sub>2</sub> (98)
V <sub>116</sub>	3026	3153	3021	8.25	vCH(100) ring
V <sub>125</sub>	3062	3189	3055	12.52	vCH(97) ring
V <sub>126</sub>	3084	3212	3077	9.02	vCH(100) thio.
V <sub>127</sub>	3106	3247	3110	4.89	vCH(99) thio.
V <sub>129</sub>	3328	3510	3363	8.73	vNH(100)

<sup>a</sup> Wavenumbers in the ranges from 4000 to 1700 cm<sup>-1</sup> and lower than 1700 cm<sup>-1</sup> are scaled with 0.958 and 0.983 for B3LYP/6-311++G(d,p) basis set, respectively.

<sup>b</sup> TED, total energy distribution; v, stretching; δ, in-plane bending, γ, out-of-plane bending; ρ, scissoring, ω, wagging; τ, torsion; r, rocking; t, twisting.

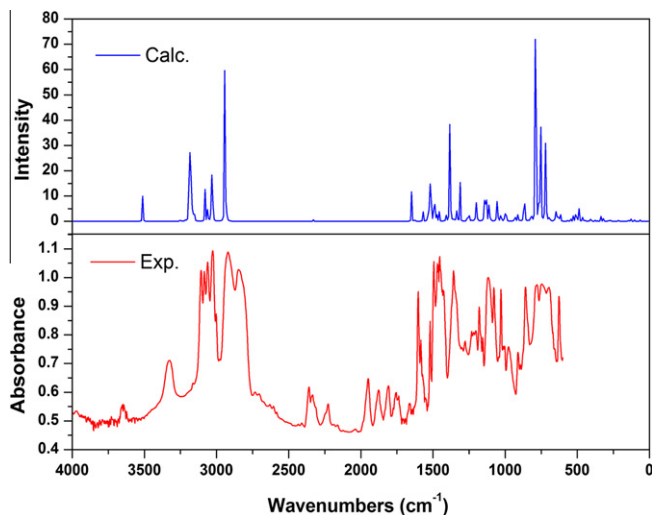


Fig. 2. The observed and calculated Infrared spectra of BPTPA.

the range 1000–1300  $\text{cm}^{-1}$  and the C–H out of plane bending vibrations occur in the frequency range 750–1000  $\text{cm}^{-1}$ . In this study, the C–H in plane and out-of-plane bending vibrations are also lie within the characteristic region. For example, the C–H in-plane bending vibrations are observed at 1078 and 1180  $\text{cm}^{-1}$  in FT-IR. The calculated frequencies are 1077 and 1179  $\text{cm}^{-1}$  that are well correlated with the experimental frequencies. The C–H out of plane bending vibrations are predicted in the region 986–843  $\text{cm}^{-1}$ . The observed frequencies (910 and 928  $\text{cm}^{-1}$ ) are coinciding very well with the calculated ones (909 and 929  $\text{cm}^{-1}$ , respectively).

The C–H (for thiophene ring) stretching vibrations are calculated at 3077, 3110 and 3114  $\text{cm}^{-1}$  and observed at 3084 and 3106  $\text{cm}^{-1}$  in FT-IR. The C–H out of plane bending of the thiophene ring were calculated at 675, 772 and 881  $\text{cm}^{-1}$  which show good agreement with value at 780  $\text{cm}^{-1}$ . According to TED, the CH in plane bending modes of thiophene ring are predicted at 1086, 1185 and 1238  $\text{cm}^{-1}$  which have major contribution.

The C–H stretching of the methylene groups are at lower frequencies than those of the aromatic C–H ring stretching. The asymmetric stretching for the  $\text{CH}_2$ ,  $\text{CH}_3$ , etc. has magnitude higher than the symmetric stretching. The  $\text{CH}_2$  asymmetric stretching vibrations are generally observed in the region 3000–2900  $\text{cm}^{-1}$ , while the  $\text{CH}_2$  symmetric stretch will appear between 2900 and 2800  $\text{cm}^{-1}$  [42,45–47]. The scissoring mode of the  $\text{CH}_2$  group gives rise to characteristic band near 1465  $\text{cm}^{-1}$  in IR spectrum [48]. In this work, the  $\text{CH}_2$  asymmetric and symmetric stretching vibrations were observed in FT-IR spectra at 2847 and 2920  $\text{cm}^{-1}$ , respectively. The calculated symmetric  $\text{CH}_2$  stretching vibrations of the methylene group were obtained at 2898, 2902  $\text{cm}^{-1}$  and the calculated asymmetric ones were obtained at 2932 and 2949  $\text{cm}^{-1}$ . The  $\text{CH}_2$  scissoring vibrations were calculated at 1487, 1484, 1464 and 1445  $\text{cm}^{-1}$ . The experimental values were assigned at 1454, 1470 and 1493  $\text{cm}^{-1}$  which show excellent agreement with calculated ones. The  $\text{CH}_2$  wagging vibrations were assigned in FT-IR at 1358, 1300 and 1278  $\text{cm}^{-1}$  that were calculated 1354, 1306 and 1284  $\text{cm}^{-1}$  which have major contribution according to TED. The  $\text{CH}_2$  twisting vibrations were observed in FT-IR at 1218 and 1232  $\text{cm}^{-1}$  which show agreement with calculated values (1225 and 1232  $\text{cm}^{-1}$ ). The rocking mode was observed at 976  $\text{cm}^{-1}$  in the infrared spectrum correlates well with scaled value at 974  $\text{cm}^{-1}$  ( $\nu_{58}$ ).

The ring carbon–carbon stretching vibrations in benzene ring occur in the region 1430–1625  $\text{cm}^{-1}$ . In general, the bands are of

variable intensity and are observed at 1625–1590, 1575–1590, 1470–1540, 1430–1465 and 1280–1380  $\text{cm}^{-1}$  from the frequency ranges given by Varsanyi [45]. In the present work, the frequencies computed at 1029–1086, 1308–1317 and 1594–1616  $\text{cm}^{-1}$  (see Table 2) were assigned as CC stretching vibrations according to TED. The TED contribution for these modes are mixed with combination of C–H in plane bending. The CC stretching vibrations were assigned at 1028, 1078, 1584 and 1602  $\text{cm}^{-1}$  in the FT-IR spectrum. The CCC in plane deformation vibrations are observed higher wavenumbers than the CCC out of plane vibrations. The theoretically calculated in-plane and out-of plane vibrations show good agreement with recorded spectral data.

The ring breathing vibrations are observed in the region 1100–1000  $\text{cm}^{-1}$ . As revealed by TED, the ring-breathing modes of the aromatic rings were calculated at 999 and 1000  $\text{cm}^{-1}$ . In FT-IR spectrum, the ring breathing vibration was observed at 1004  $\text{cm}^{-1}$ . The ring assignments proposed in this study are also in agreement with the literature values [22,30,40,42].

The C–C stretching modes were observed at 1516  $\text{cm}^{-1}$  mode for 3-ethynylthiophene [49]. This peak was observed at 1428 and 1520  $\text{cm}^{-1}$  in FT-IR spectrum and calculated at 1426 and 1537  $\text{cm}^{-1}$ .

The  $\text{C}\equiv\text{C}$  modes, its position is highly characteristic, arise from conjugation and from aromatic substitutions are also very informative. The  $\text{C}\equiv\text{C}$  mode of the compound was calculated and observed the same value, at 2228  $\text{cm}^{-1}$ . It is evident of TED value contributing to 100%. Also this mode is very good agreement with the literature [50].

Identification of C–S stretching vibration is difficult and also uncertain. The recorded four peaks which are 608.8, 753.5, 839.5, and 872.8  $\text{cm}^{-1}$  were assigned to C–S stretching by [14,15] according to potential energy distribution (PED) obtained from DFT calculations. Coruh et al. [16] assigned this mode at 834  $\text{cm}^{-1}$  in FT-IR spectrum. In this study, we have assigned three C–S stretching modes, based on TED calculations; this mode recorded in FT-IR spectra at 858  $\text{cm}^{-1}$ . The C–S stretching modes are calculated at 641, 846 and 848  $\text{cm}^{-1}$  have dominant contribution assigned by TED.

The remainder of the observed and calculated wavenumbers and assignments of present molecule are shown in Table S1.

The correlation graphic which described harmony between the calculated and experimental wavenumbers (Supp. Material Fig. S1). As can be seen from Fig. S1, experimental fundamentals have a good correlation with B3LYP. The relations between the calculated and experimental wavenumbers are linear and described by the following equation:

$$\nu_{\text{cal.}} = 1.0015\nu_{\text{exp.}} - 2.7481 \quad (R^2 = 0.9999)$$

As a result, the scaled fundamental vibrational are in good consistency with the experimental results and are found a good agreement above the predicated literature.

#### NMR spectra

Experimental  $^1\text{H}$ ,  $^{13}\text{C}$  and APT NMR spectra were recorded as shown in Figs. 3–5. The  $^{13}\text{C}$  and  $^1\text{H}$  theoretical chemical shifts and the assignments of BPTPA are presented in Table 3, according to the Fig. 1 atom positions. Firstly, full geometry optimization of BPTPA was performed at the gradient corrected density functional level of theory using the hybrid B3LYP method based on Becke's three parameters. Then, gauge-invariant atomic orbital (GIAO)  $^1\text{H}$  and  $^{13}\text{C}$  chemical shift calculations of the compound was done by same method using 6-311++G(d,p) basis set IEFPCM/chloroform solution. Application of the GIAO [51] approach to molecular systems was significantly improved by an efficient application of the

method to the ab initio SCF calculation, using techniques borrowed from analytic derivative methodologies. Relative chemical shifts were estimated by using the corresponding TMS shielding calculated in advance at the same theoretical level as the reference. The  $^1\text{H}$  and  $^{13}\text{C}$  NMR spectra were taken in chloroform by using IEFPCM method [52].

In this study, there are twenty-two carbon signals calculated theoretically of which are sixteen aromatic carbon signals. The twelve aromatic carbon signals out of sixteen aromatic carbons were only observed experimentally in the  $^{13}\text{C}$  spectrum of the molecule, due to the symmetry of two phenyl rings. In contrast to carbon signals, twenty-one proton signals were calculated while twenty protons were observed in the  $^1\text{H}$  spectrum according to integration. The proton which is calculated at 1.16 ppm ( $\text{H}_{29}$ ) is not observed in the  $^1\text{H}$  spectrum. The chemical shifts of NH protons in generally would be more susceptible to intermolecular interactions as compared other heavier atoms. Therefore the N–H proton signal varies greatly with concentration and solvent effects and occasionally can't be seen in the spectra [53].

In general, chemical shifts for the protons of organic molecules vary greatly with the electronic environment of the proton. Hydrogen attached or nearby electron-withdrawing atom or group can decrease the shielding and move the resonance of attached proton towards to a higher frequency. By contrast electron-donating atom or group increases the shielding and moves the resonance towards to a lower frequency [54]. The chemical shifts of aromatic protons of organic compounds are usually observed in the range of 7.00–8.00 ppm, while aliphatic protons resonance in the high field. The signals of the thirteen aromatic proton ( $^1\text{H}$ ) of the title compound were calculated theoretically 7.13–7.96 ppm, observed at 7.08–7.35 ppm experimentally. We predicted  $\text{H}_{36}$  at 7.96 ppm in the lowest field, and  $\text{H}_{32}$  at 7.13 ppm in the highest field of the aromatic region. These protons are observed at 7.35 and 7.08 ppm, respectively. Other eleven aromatic protons are accumulated in

the range of 7.33–7.69 ppm, observed experimentally at 7.19–7.30 ppm. The protons resonance in this region could not be assigned unambiguously one by one due to overcrowding experimentally. It is very interesting to note that despite the protons ( $\text{H}_{32}$ ,  $\text{H}_{36}$ ) of the molecule are expected to be symmetrical, the proton ( $\text{H}_{32}$ ) facing to the other phenyl ring is to have experienced different magnetic environment than  $\text{H}_{36}$ , as suggested by the theoretical and experimental results, thereby leading to the observation of the proton ( $\text{H}_{32}$ ) at a reduced chemical shift compared to the other one. The origin of this phenomenon could be somewhat attributable to the molecular dynamics of this relatively complex molecule.

The aliphatic seven protons were calculated in the region of 2.36–4.03 ppm, observed in 2.48–3.89 ppm. Benzylic protons were predicted at 4.03 ( $\text{H}_{30}$ ) and 3.00 ( $\text{H}_{31}$ ) ppm, observed at 3.89 and 3.81 ppm, respectively. Methine proton ( $\text{H}_{26}$ ) was calculated 2.94 ppm, observed as quintet at 3.04 ppm showing a good agreement. Methylene protons ( $\text{H}_{24}$ ,  $\text{H}_{25}$ ) of the molecule were predicted at 3.63 and 2.36 ppm and observed as multiplet in 2.85–2.93 ppm. The methylene protons ( $\text{H}_{28}$ ,  $\text{H}_{27}$ ) next to the triple bond were calculated at 3.21 and 2.36 ppm, respectively, while observed as two different doublet of doublets at 2.54 and 2.48 ppm. Overall, the calculated protons chemical shifts of the molecule show fairly good correlation to the experimental spectrum.

Aromatic carbons give signals in overlapped areas of the spectrum with chemical shift values ranging from 100 to 150 ppm [53,55]. The sixteen aromatic carbons were calculated in the region of 126.57–148.11 ppm theoretically, observed signals are in the range of 122.96–140.62 ppm. Aromatic carbon chemical shifts (*ipso*-carbons  $\text{C}_4$ ,  $\text{C}_{13}$ ) were calculated at 148.11 and 147.83 ppm, observed at 140.62 and 139.19 ppm. The lowest signal of the aromatic carbons atom  $\text{C}_{37}$  was predicted at 126.57 ppm and observed 122.96 ppm according to  $^{13}\text{C}$  and APT NMR spectrum. The other phenyl and thiophene ring carbon chemical shifts (thirteen aro-

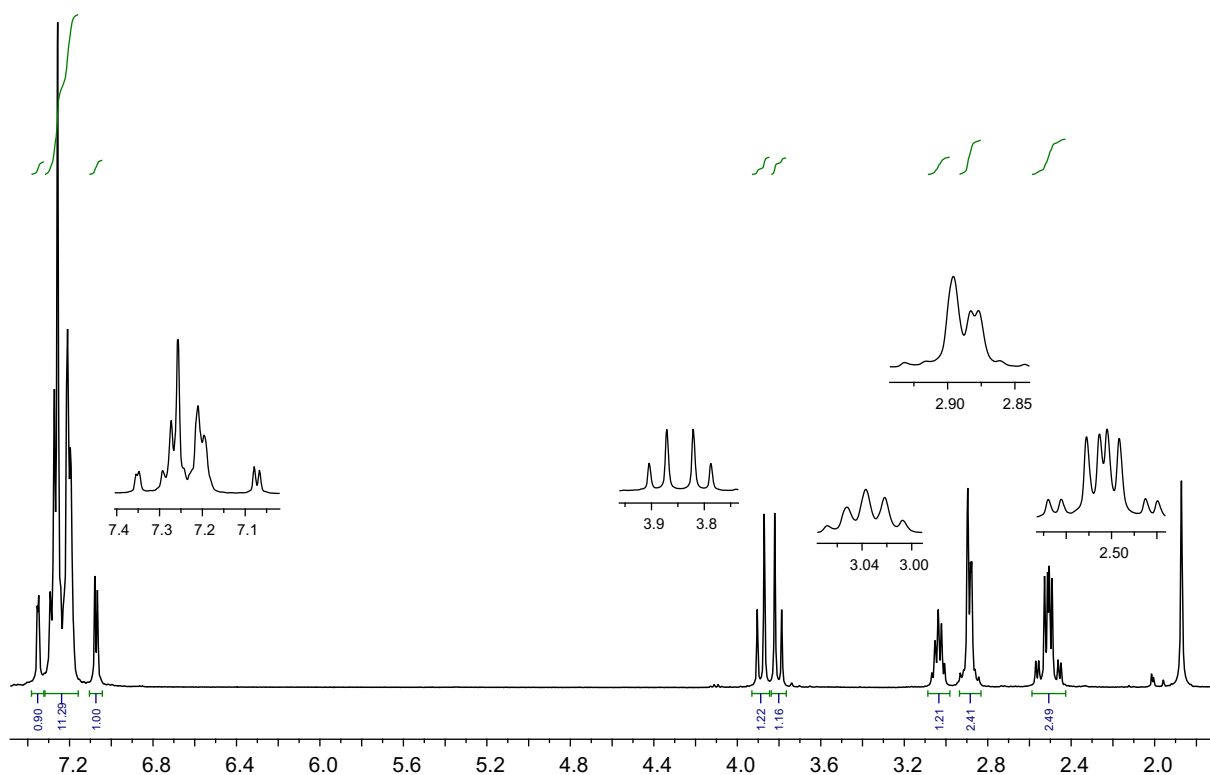


Fig. 3. The experimental  $^1\text{H}$  NMR spectra of BPTPA.

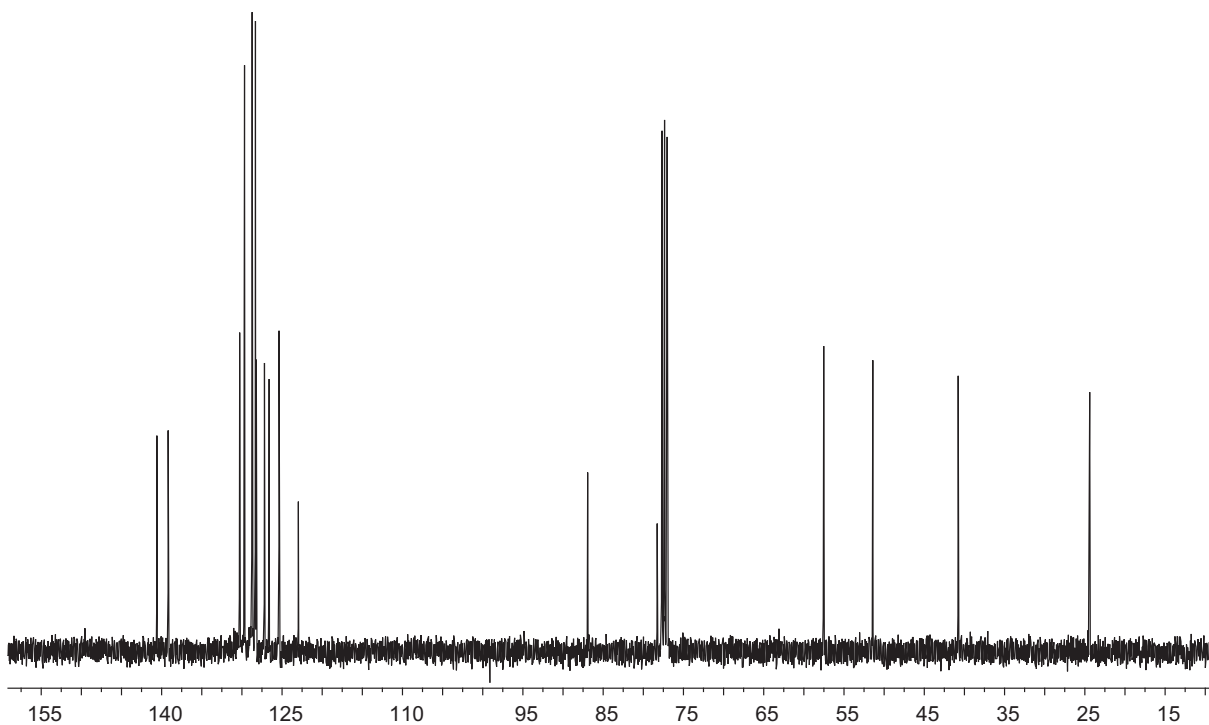


Fig. 4. The experimental  $^{13}\text{C}$  NMR spectra of BPTPA.

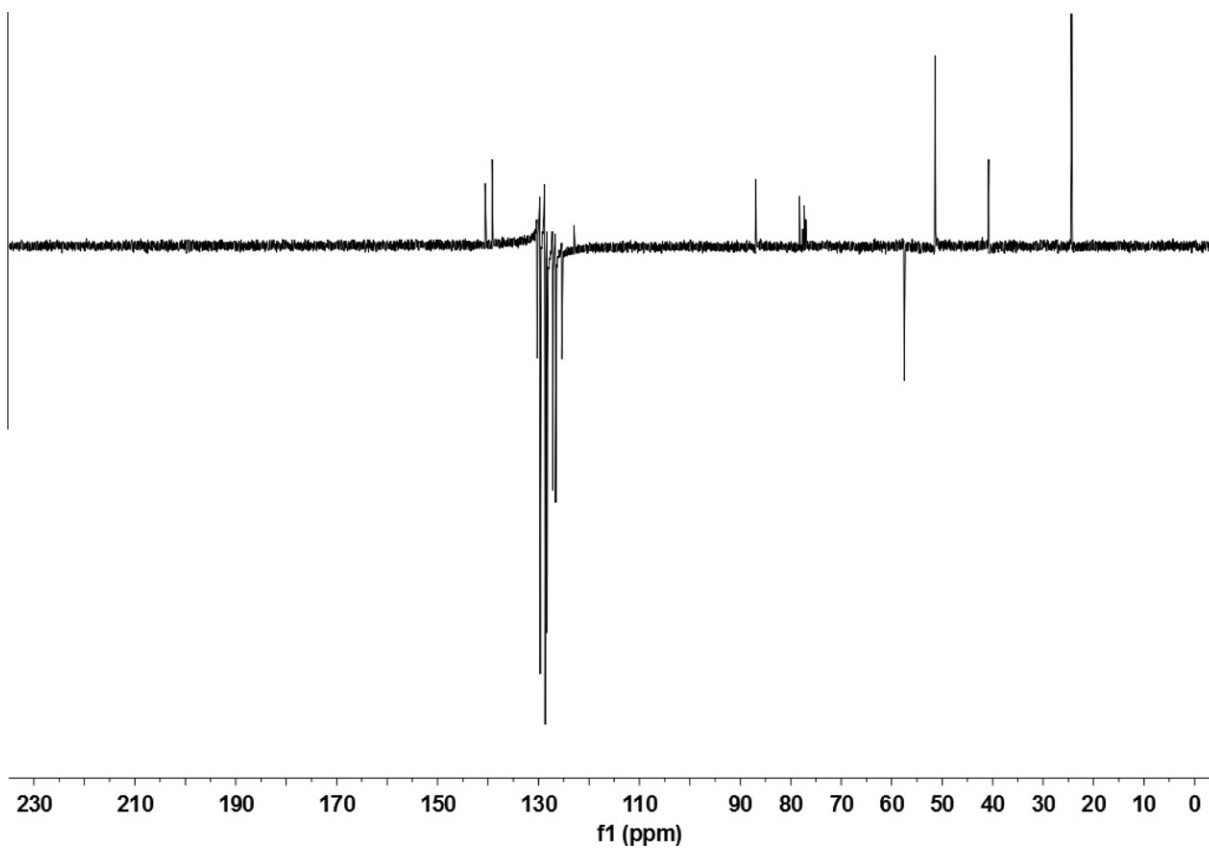


Fig. 5. The experimental APT NMR spectra of BPTPA.

matic carbons) were observed in the range of 125.34–130.27 ppm and calculated in the range of 130.54–140.42 ppm, showing a good correlation as seen in Table 3. Aliphatic carbons were observed in

the region of 20–90 ppm. Triple bond carbons were resonanced at 86.92 ( $\text{C}_{10}$ ) and 78.23 ppm ( $\text{C}_{45}$ ) and the chemical shifts of these carbons were calculated at 93.91 and 80.23 ppm, respectively.

**Table 3**Experimental and theoretical  $^1\text{H}$  and  $^{13}\text{C}$  NMR isotropic chemical shifts (with respect to TMS) of BPTPA by DFT B3LYP method.

Atom	B3LYP	Exp. <sup>a</sup>	Atom	B3LYP	Exp. <sup>a</sup>
C <sub>13</sub>	148.11	139.19/140.62	C <sub>8</sub>	67.74	57.52
C <sub>4</sub>	147.83	140.62/139.19	C <sub>12</sub>	56.12	51.42
C <sub>39</sub>	140.42	125.34–130.27	C <sub>7</sub>	44.57	40.78
C <sub>40</sub>	135.88	125.34–130.27	C <sub>9</sub>	26.54	24.39
C <sub>38</sub>	134.71	125.34–130.27	H <sub>36</sub>	7.96	7.35
C <sub>3</sub>	134.34	125.34–130.27	H <sub>22</sub>	7.69	7.19–7.30
C <sub>6</sub>	134.24	125.34–130.27	H <sub>35</sub> ,H <sub>23</sub> ,H <sub>43</sub>	7.56	7.19–7.30
C <sub>18</sub>	134.17	125.34–130.27	H <sub>19</sub> ,H <sub>21</sub> ,H <sub>41</sub> ,H <sub>33</sub> ,H <sub>44</sub> ,H <sub>20</sub> ,H <sub>34</sub>	7.33	7.19–7.30
C <sub>2</sub>	133.42	125.34–130.27	H <sub>32</sub>	7.13	7.08
C <sub>5</sub>	133.24	125.34–130.27	H <sub>30</sub>	4.03	3.89/3.81
C <sub>14</sub>	133.05	125.34–130.27	H <sub>24</sub>	3.63	2.85–2.93
C <sub>17</sub>	132.93	125.34–130.27	H <sub>28</sub>	3.21	2.48/2.54
C <sub>15</sub>	132.68	125.34–130.27	H <sub>31</sub>	3.00	3.89/3.81
C <sub>16</sub>	131.42	125.34–130.27	H <sub>26</sub>	2.94	3.04
C <sub>1</sub>	130.54	125.34–130.27	H <sub>25</sub>	2.36	2.85–2.93
C <sub>37</sub>	126.57	122.96	H <sub>27</sub>	2.36	2.48/2.54
C <sub>10</sub>	93.91	86.92	H <sub>29</sub>	1.16	–
C <sub>45</sub>	80.23	78.23			

<sup>a</sup> / sign mean: or and – sign mean: signal of range.**Table 4**The experimental and computed absorption wavelength  $\lambda$  (nm), excitation energies  $E$  (eV), absorbance and oscillator strengths ( $f$ ) of BPTPA using TD-DFT/6-311G++(d, p).

	Experimental			B3LYP			
	$\lambda$ (nm)	Energy (eV)		$\lambda$ (nm)	Energy (eV)	Osc. strength ( $f$ )	Major contribution ( $\geq 10\%$ )
Water	277	4.482	Water	260	4.769	0.2833	HOMO $\rightarrow$ LUMO (91%)
	287	4.326		248	5.000	0.0931	HOMO–1 $\rightarrow$ LUMO (91%)
Ethanol	278	4.460	Ethanol	260	4.769	0.2886	HOMO $\rightarrow$ LUMO (91%)
	287	4.321		249	4.980	0.0910	HOMO–1 $\rightarrow$ LUMO (91%)
Chloroform	279	4.444	Chloroform	260	4.769	0.3055	HOMO $\rightarrow$ LUMO (92%)
	286	4.336		249	4.980	0.0811	HOMO–1 $\rightarrow$ LUMO (92%)
			Gas	277	4.482	0.4056	HOMO $\rightarrow$ LUMO (92%)
			297	4.180	0.0020	HOMO–6 $\rightarrow$ LUMO (94%)	

Methine and methylene carbons were calculated at 67.74 (C<sub>8</sub>), 56.12 (C<sub>12</sub>), 44.57 (C<sub>7</sub>) and 26.54 (C<sub>9</sub>) using by the B3LYP method and observed at 57.52, 51.42, 40.78 and 24.39 ppm, respectively, as evident from  $^{13}\text{C}$  and APT spectra.

#### Molecular electrostatic potential, electronic structure and UV spectra

The calculations of the electronic structures of the title compound were carried out using TD-DFT calculations with the B3LYP/6-311++G(d,p) method. Before the electronic calculations, the molecule was optimized in ground state using the DFT method with B3LYP functional. It is obvious that the use of TD-DFT calculations for prediction of the electronic absorption spectra is a reasonable method. The theoretical and experimental maximum absorption wavelengths, excitation energies, absorbance and oscillator strengths are collected in Table 4.

The energies of the some molecular orbitals such as NH, CH<sub>2</sub>, C $\equiv$ C, phenyl and thiophene groups were individually studied with respect to the percentage contribution of the each species to the total energy of the compound. The molecular orbital of phenyl and thiophene rings contain significant contribution to the BPTPA. Two phenyl rings have 100% contribution to the LUMO of the molecule, while significant contributions to the HOMO of the compound comes from the thiophene (48%) and C $\equiv$ C groups (29%).

The TDOS, PDOS and OPDOS or COOP density of states [56,57], in terms of Mulliken population analysis were calculated and created by convoluting the molecular orbital information with Gauss-

ian curves of unit height and FWHM (Full Width at Half Maximum) of 0.3 eV using Gausssum2.2 [58]. Because of the results from multiplying DOS by the overlap population, the COOP is similar to DOS. The TDOS, PDOS and COOP spectra are plotted in Figs. 6–8, respectively. The most important application of the DOS plot is to demonstrate MO (molecule orbital) compositions and their contributions

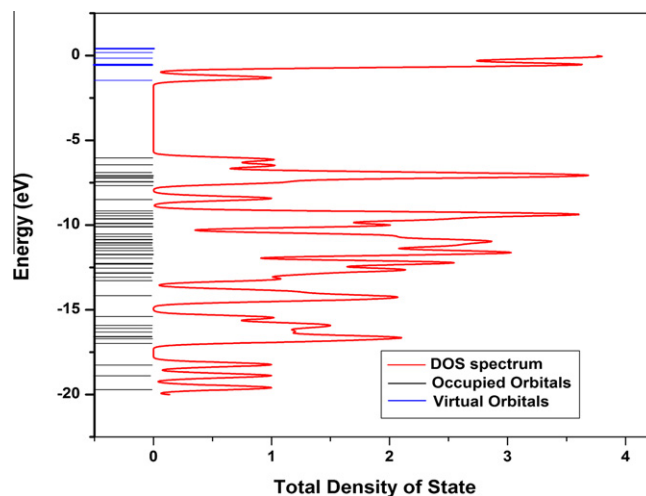


Fig. 6. Calculated total electronic density of states for BPTPA.

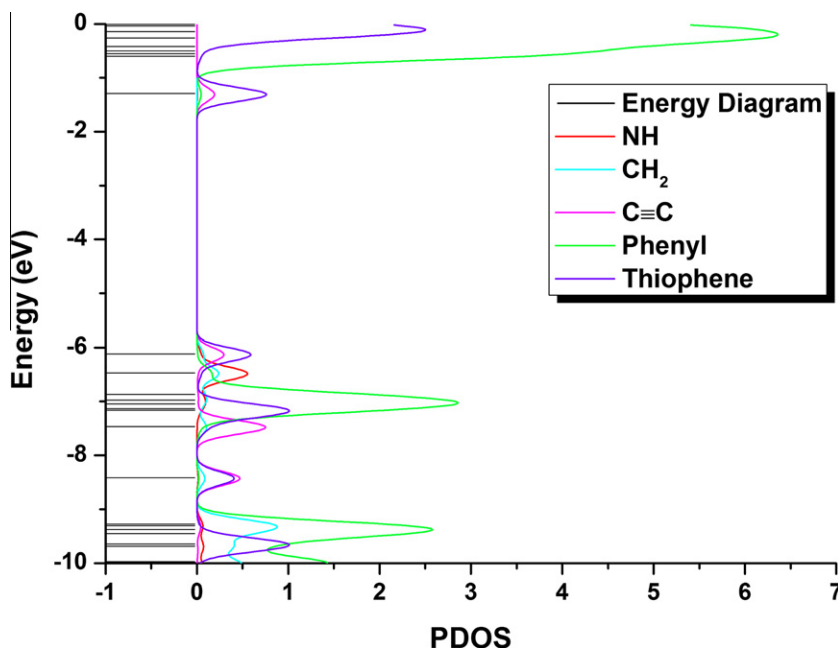


Fig. 7. Calculated partial electronic density of states for BPTPA.

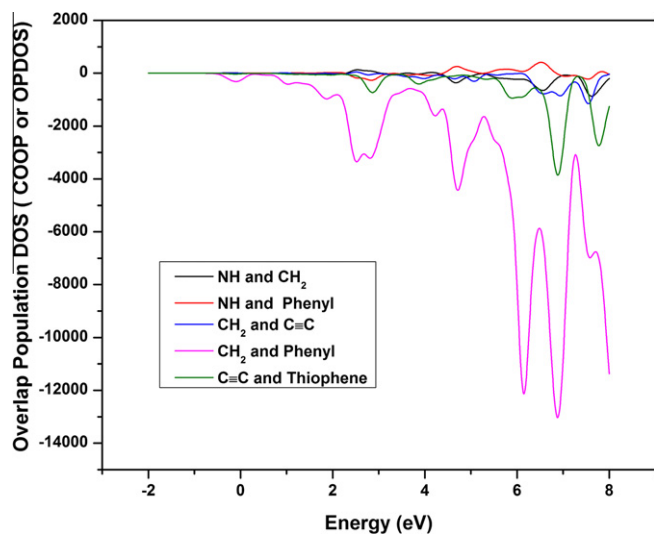


Fig. 8. Overlap population DOS curves of BPTPA.

to chemical bonding through the OPDOS plots which are also referred in the literature as Crystal Orbital Overlap Population (COOP) diagrams. The COOP shows the bonding, anti-bonding and nonbonding interaction of the two orbitals, atoms or groups. A positive value of the COOP indicates a bonding interaction, however negative value means an anti-bonding interaction and zero value indicates nonbonding interactions [59]. The PDOS mainly presents the composition of the fragment orbitals contributing to the molecular orbitals as seen from Fig. 6. The PDOS of phenyl and thiophene groups is of very similar nature of state as in the TDOS of BPTPA because of the higher energies than the other groups, in terms of the extent of the contribution to the energy of the molecular orbitals. The OPDOS or COOP diagrams were presented in Fig. 7. It is readily seen in Fig. 7 that the interaction between C≡C and thiophene (green line) system was seen as a negative (anti-bonding interaction) as well as CH<sub>2</sub> ↔ benzenes

and CH<sub>2</sub> ↔ C≡C systems for the states in energy window from –0.58 to 7.99 eV. One can see nonbonding states; C≡C ↔ thiophene, CH<sub>2</sub> ↔ phenyls and CH<sub>2</sub> ↔ C≡C systems in the ranges of –1.6 to 0.5, –1.92 to –0.47 and –0.27 to 1.08 eV, respectively. The OPDOS or COOP diagrams also showed that the NH ↔ CH<sub>2</sub> and NH ↔ Phenyls have significant bonding characters which are of positive value. Their energy values were calculated in the range of 2.31–3.10, 4.01–4.23 eV for the NH ↔ CH<sub>2</sub> and 1.1–2.29, 4.39–6.84 and 7.74–7.79 eV for NH ↔ Phenyls (bonding interactions).

HOMO and LUMO are the main orbital taking part in chemical reaction. The HOMO energy characterizes the ability of electron giving, and the LUMO accepting, and the gap between HOMO and LUMO characterizes the molecular chemical stability [60]. The energy gap between HOMO and LUMO is a critical parameter in determining molecular electrical transport properties due to the measurement of electron conductivity. As seen Fig. 9, the HOMO of the title compound presents a charge density localized on the thiophene, C≡C and CH groups and LUMO is characterized by a charge distribution on the two phenyl rings. The energy value of HOMO was computed at –0.298 and LUMO is –0.167 a.u., and the energy gap was calculated 0.131 a.u. The energy gap between HOMO and LUMO explains the chemical reactivity, optical polarizability, kinetic stability and chemical softness–hardness of a molecule. The chemical hardness is a good indicator of the chemical stability. The molecules having a small energy gap are known as soft and having a large energy gap are known as hard molecules. The hard molecules are not more polarizable than the soft ones because they need big energy to excitation [61]. The hardness ( $\eta$ ) value of a molecule is formulated by the following equation [62].

$$\eta = \frac{(-\varepsilon_{\text{HOMO}} + \varepsilon_{\text{LUMO}})}{2}$$

where  $\varepsilon_{\text{HOMO}}$  and  $\varepsilon_{\text{LUMO}}$  are the energies of the HOMO and LUMO orbitals. The value of energy gap between the HOMO and LUMO is 3.55656 eV and the value of hardness is 1.77828 eV for the title molecule. The chemical hardness value is a little bit smaller than that of (E)-4-methoxy-2-[(*p*-tolylimino)methyl]phenol molecule [61], which is a Schiff based compound (1.842 eV), that is a hardness molecule.

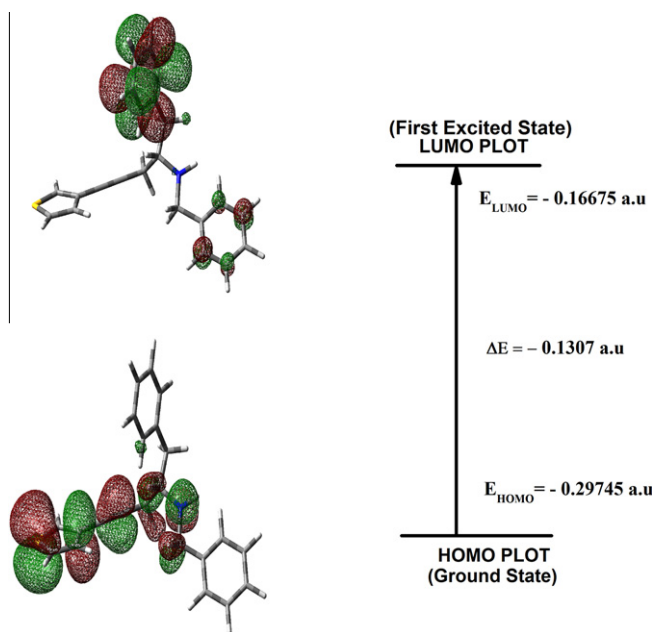


Fig. 9. The frontier and second frontier molecular orbitals of BPTPA.

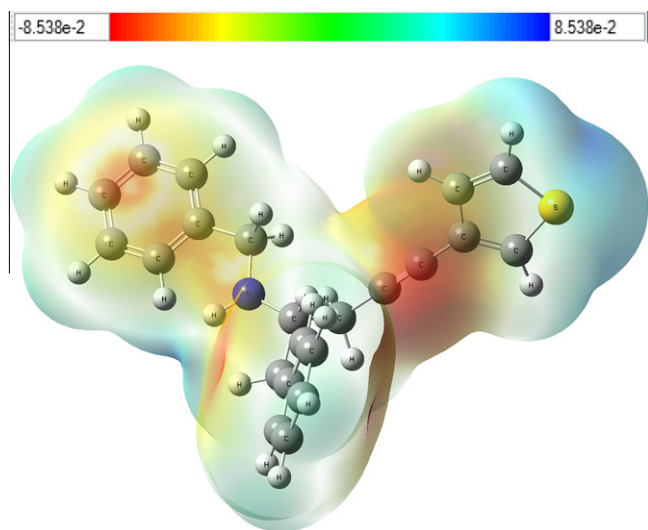


Fig. 10. Molecular electrostatic potential map (MEP) of BPTPA.

The maximum absorption values were observed at 277 and 287, 278 and 287, 279 and 286 nm in water, ethanol and chloroform, respectively. Calculated  $\lambda_{\text{max}}$  values obtained with B3LYP/6-311++G(d,p) are 260 and 248 nm in water which are HOMO  $\rightarrow$  LUMO and HOMO-6  $\rightarrow$  LUMO transition, respectively. In ethanol and chloroform, these values are calculated at 260 and 248 nm which are the same transition in water (see Table 4).

In the present study, 3D plots of molecular electrostatic potential (MEP) of BPTPA is illustrated in Fig. 10. The MEP which is a plot of electrostatic potential mapped onto the constant electron density surface with together HOMO and LUMO (Fig. 11). The MEP is a useful property to study reactivity given that an approaching electrophile will be attracted to negative regions (where the electron distribution effect is dominant). The importance of MEP lies in the fact that it simultaneously displays molecular size, shape as well as positive, negative and neutral electrostatic potential re-

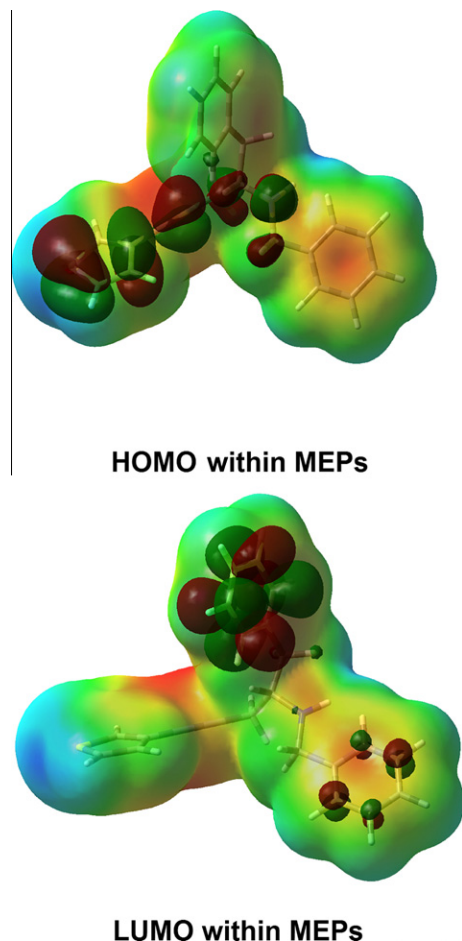


Fig. 11. Molecular electrostatic potential surface (MEPs) with in HOMO and LUMO of BPTPA.

gions in terms of color grading (Figs. 10 and 11) and is very useful in research of molecular structure with its physiochemical property relationship [63,64]. The different values of the electrostatic potential at the surface are represented by different colors. Potential increases in the order red < orange < yellow < green < blue. The color code of these maps is in the range between  $-0.08538$  a.u. (deepest red) to  $0.08538$  a.u. (deepest blue) in compound, where blue indicates the strongest attraction and red indicates the strongest repulsion. MEPs color scale is such  $\delta^+ \rightarrow \delta^-$  in the direction red  $\rightarrow$  blue. As can be seen from the MEP map of the title molecule, while regions having the negative potential are over the electronegative atoms (C $\equiv$ C group and Nitrogen atom), the regions having the positive potential are over the sulfur and hydrogen atoms. The negative potential value is  $-0.0952076$  a.u. for the C $\equiv$ C group. A maximum positive region localized on the S atom bond has value of  $+0.0708951$  a.u. From this results, we can say that the S atom indicates the strongest attraction and C $\equiv$ C group indicates the strongest repulsion.

#### Nonlinear optical (NLO) effects

NLO properties has been of great interest by the recent years. Because some synthesized novel materials show efficient nonlinear optical that are used telecommunication, potential applications in modern communication technology, optical signal processing and data storage.

In this study, the electronic dipole moment, molecular polarizability, anisotropy of polarizability and molecular first hyperpolar-

izability of present compound were investigated. The polarizability and hyperpolarizability tensors ( $\alpha_{xx}, \alpha_{xy}, \alpha_{yy}, \alpha_{xz}, \alpha_{yz}, \alpha_{zz}$  and  $\beta_{xxx}, \beta_{xxy}, \beta_{xyy}, \beta_{yyy}, \beta_{xxz}, \beta_{xyx}, \beta_{yxx}, \beta_{xzz}, \beta_{yzz}, \beta_{zzz}$ ) can be obtained by a frequency job output file of Gaussian. However,  $\alpha$  and  $\beta$  values of Gaussian output are in atomic units (a.u.) so they have been converted into electronic units (esu) ( $\alpha$ ; 1 a.u. =  $0.1482 \times 10^{-24}$  esu,  $\beta$ ; 1 a.u. =  $8.6393 \times 10^{-33}$  esu). The mean polarizability ( $\alpha$ ), anisotropy of polarizability ( $\Delta\alpha$ ) and the average value of the first hyperpolarizability ( $\beta$ ) can be calculated using the below equations.

$$\alpha_{tot} = \frac{1}{3}(\alpha_{xx} + \alpha_{yy} + \alpha_{zz})$$

$$\Delta\alpha = \frac{1}{\sqrt{2}}[(\alpha_{xx} - \alpha_{yy})^2 + (\alpha_{yy} - \alpha_{zz})^2 + (\alpha_{zz} - \alpha_{xx})^2 + 6\alpha_{xz}^2 + 6\alpha_{xy}^2 + 6\alpha_{yz}^2]^{\frac{1}{2}}$$

$$\langle\beta\rangle = [(\beta_{xxx} + \beta_{xyy} + \beta_{xzz})^2 + (\beta_{yyy} + \beta_{yzz} + \beta_{yxx})^2 + (\beta_{zzz} + \beta_{zxx} + \beta_{zyy})^2]^{\frac{1}{2}}$$

In Table 5, the calculated parameters described above and electronic dipole moment  $\{\mu_i (i = x, y, z)\}$  and total dipole moment  $\mu_{tot}$  for title compound are listed. The total dipole moment can be calculated using the following equation.

$$\mu_{tot} = (\mu_x^2 + \mu_y^2 + \mu_z^2)^{\frac{1}{2}}$$

It is well known that the higher values of dipole moment, polarizability, and hyperpolarizability are important for more active NLO properties. The calculated dipole moment is equal to 0.404117 Debye (D). The highest value of dipole moment is observed for component  $\mu_z$ . In this direction, this value is equal to 0.388142 D. Total polarizability ( $\alpha_{tot}$ ) and anisotropy of polarizability ( $\Delta\alpha$ ) are calculated as 43.094626 and 102.972128 esu. The first hyperpolarizability value  $\beta_{tot}$  of the title compound is equal to  $18.622910 \times 10^{-31}$  esu. The hyperpolarizability  $\beta$  was dominated by the longitudinal components of  $\beta_{xxx}$ . Domination of particular component indicates on a substantial delocalization of charges in this direction.

The polarizability and the first hyperpolarizability of title molecule is ca. 10 and 2 times greater than those of urea ( $\alpha$  and  $\beta$  of urea are  $9.868774 \times 10^{-24}$ , and  $7.803240 \times 10^{-31}$  esu obtained by B3LYP/6-311++G(d,p) method. That is to say, the title compound can be used as a good candidate of NLO materials.

**Mulliken atomic charges**

The computed of reactive atomic charges plays an important role in the application of quantum mechanical calculations the molecular system. The Mulliken atomic charges of title molecule is presented in Table 6 and shown in Fig. 12. The Mulliken atomic

**Table 5**  
The dipole moments  $\mu$  (D), the polarizability  $\alpha$  (a.u.), the average polarizability  $\alpha_o$  (esu), the anisotropy of the polarizability  $\Delta\alpha$  (esu), and the hyperpolarizability  $\beta$  (esu) of BPTPA.

$\mu_x$	-0.058481	$\beta_{xxx}$	206.904023
$\mu_y$	0.096105	$\beta_{xxy}$	-55.934514
$\mu_z$	-0.388142	$\beta_{xyy}$	-33.644834
$\mu_o$	0.404117	$\beta_{yyy}$	143.272517
$\alpha_{xx}$	391.485183	$\beta_{xxx}$	64.436064
$\alpha_{xy}$	-30.016936	$\beta_{xyz}$	-46.976706
$\alpha_{yy}$	232.783937	$\beta_{yyz}$	-59.576790
$\alpha_{xz}$	3.844925	$\beta_{xzz}$	20.290236
$\alpha_{yz}$	-9.629177	$\beta_{yzz}$	-4.205349
$\alpha_{zz}$	248.091735	$\beta_{zzz}$	-50.618112
$\alpha_{total}$	43.094626	$\beta_x$	193.549424
$\Delta\alpha$	102.972128	$\beta_y$	83.132654
		$\beta_z$	-45.758839
		$\beta$	18.622910

**Table 6**  
Mulliken atomic charges of BPTPA.

C1	-0.410936	H19	0.154479
C2	-0.225112	H20	0.179973
C3	-0.241833	H21	0.174833
C4	0.857943	H22	0.163873
C5	-0.060981	H23	0.179023
C6	-0.279943	H24	0.171741
C7	-1.075578	H25	0.179203
C8	-0.187034	H26	0.158184
C9	-0.216641	H27	0.191107
C10	0.038056	H28	0.148431
C12	-0.872355	H29	0.091043
C13	1.078712	H30	0.144600
C14	-0.319091	H31	0.133513
C15	-0.256026	H32	0.150598
C16	-0.399857	H33	0.174981
C17	-0.310507	H34	0.152493
C18	-0.095033	H35	0.178346
C37	-0.715620	H36	0.168712
C38	-1.109054	H41	0.161396
C39	1.201769	H43	0.258678
C40	0.280355	H44	0.284591
C45	-0.715620	N11	0.178015
S42	-0.575821		

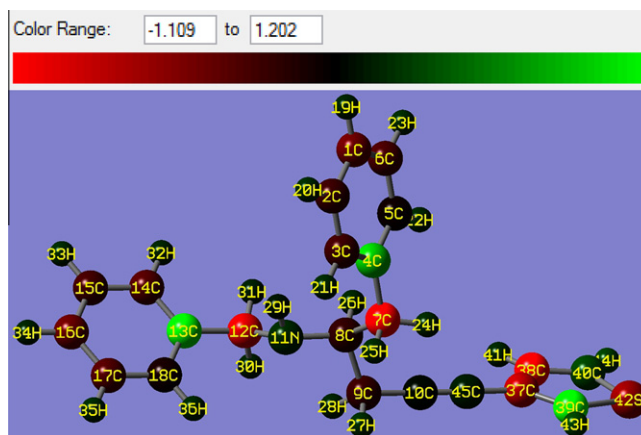


**Fig. 12.** Mulliken atomic charge distribution of BPTPA.

charges are computed by the DFT/B3LYP method 6-311++G(d,p) basis set.

As can be seen in Table 6, all hydrogen atoms and N atom have a net positive charge. The maximum negative charge C38, C7, C12, C37, C45 and sulfur atom which are donor atoms and net positive charge on hydrogen and nitrogen atoms, which are acceptor atoms. The donor and acceptor atoms may suggest the presence of both inter-molecular hydrogen bonding in the crystalline phase.

**Conclusions**

The novel compound (S)-N-benzyl-1-phenyl-5-(thiophen-3-yl)-4-pentyn-2-amine was synthesized for the first time and several spectroscopic properties were studied using experimental techniques (FT-IR, NMR and UV) and tools derived from the density functional theory. The optimized geometric parameters of molecule were interpreted and compared with structurally similar compounds. The vibrational FT-IR spectrum of molecule was recorded. The computed vibrational wavenumbers were assigned and compared with experimental values. The magnetic properties of the title compound were calculated and compared with the experimental data which are obtained from <sup>1</sup>H and <sup>13</sup>C NMR spectra. The TDOS, PDOS and OPDOS diagrams were presented and

interpreted. Some of the groups such as phenyl and thiophene rings contribute similarly to the TDOS of BTPA. The OPDOS diagrams showed interactions for five groups and  $C\equiv C \leftrightarrow$  thiophene have significant anti-bonding character. The electronic absorption properties were also calculated and experimental electronic spectrum was recorded. Furthermore, the polarizability, first hyperpolarizability and total dipole moment of title molecule were calculated and the results are discussed. These results indicate that the studied compound is a good candidate of nonlinear optical materials. We hope that the results of this study will help researchers to synthesis of new materials.

## Appendix A. Supplementary data

Supplementary data associated with this article can be found, in the online version, at <http://dx.doi.org/10.1016/j.saa.2012.05.087>.

## References

- [1] H.J. Bertram, R. Emberger, M. Guntrt, H. Sommer, P. Werkhoff, *Recent Dev. Flavor Frag. Chem.* 11 (1993) 241–259.
- [2] J.B. Press, *Chem. Heterocycl. Compd.* 44 (1991) 397–502.
- [3] D. Bloor, *Chem. Ber.* 31 (1995) 385–387.
- [4] H.S. Nalwa, *Adv. Mater.* 5 (1993) 341–358.
- [5] I.Y. Wu, J.T. Lin, Ch.S. Li, W.C. Wang, T.H. Huang, Y.S. Wen, T. Chow, Ch. Tsai, *Tetrahedron* 55 (1999) 13973–13982.
- [6] V.P. Rao, A.K.Y. Jen, Y.J. Cai, *Chem. Soc. Chem. Commun.* 10 (1996) 1237–1238.
- [7] M. Irie, *Chem. Rev.* 100 (2000) 1685–1716.
- [8] G.Ch. Barbarella, *Eur. J. J* 8 (2002) 5072–5077.
- [9] T. Nishiumi, M. Higuchi, K. Yamamoto, *Macromolecules* 36 (2003) 6325–6332.
- [10] M. Heeney, S. Tierney, I. McCulloch, S. Higgins, D. Crouch, P. Skabara, *European Patent (Patent applicant)* 1 (2005) 1.
- [11] G. Barbarella, M. Zambianchi, *Tetrahedron* 50 (1994) 11249–11256.
- [12] J.S. Kwiatkowski, J. Leszczynski, I. Teca, *J. Mol.* 451 (1997) 436–437.
- [13] F.J. Ramirez, V. Hernandez, J.T. Lopez Navarrete, *J. Compt. Chem.* 15 (1994) 405–423.
- [14] T.D. Klots, R.D. Chirico, W.V. Steele, *Spectrochim. Acta A* 50 (1994) 765–795.
- [15] D.K. Singh, S.K. Srivastava, A.K. Ojha, B.P. Asthana, *J. Mol. Struct.* 892 (2008) 384–391.
- [16] A. Coruh, F. Yilmaz, B. Sengez, M. Kurt, M. Cinar, M. Karabacak, *Struct. Chem.* 22 (2011) 45–56.
- [17] M. Rico, J.M. Orza, J. Morcillo, *Spectrochim. Acta* 21 (1965) 689–719.
- [18] M.A. Palafox, G. Tardajos, A.G. Martinez, V.K. Rastogi, D. Mishra, S.P. Ojha, W. Kiefer, *Chem. Phys.* 340 (2007) 17–31.
- [19] M. Karabacak, E. Kose, M. Kurt, *J. Raman Spectrosc.* 41 (2010) 1085–1097.
- [20] Z. Meng, W.R. Carper, *J. Mol. Struct. Theochem.* 588 (2002) 45–53.
- [21] A. Atac, M. Karabacak, C. Caglar, E. Kose, *Spectrochim. Acta A* 85 (2012) 145–154.
- [22] A.M. Asiri, M. Karabacak, M. Kurt, K.A. Alamry, *Spectrochim. Acta A* 82 (2011) 444–455.
- [23] P. Hohenberg, W. Kohn, *Phys. Rev.* 136 (1964) B864–B871.
- [24] A.D. Becke, *J. Chem. Phys.* 98 (1993) 1372–1377.
- [25] C. Lee, W. Yang, R.G. Parr, *Phys. Rev. B* 37 (1988) 785–789.
- [26] M. Eskici, A. Karanfil, M.S. Ozer, C. Sarikurkcu, *Tetrahedron Lett.* 52 (2011) 6336–6341.
- [27] A.J. Williams, S. Chaktong, S. Gray, R.M. Lawrence, T. Gallagher, *Org. Lett.* 5 (2003) 811–814.
- [28] M.J. Frisch et al., *GAUSSIAN 09*, Revision A.1, Gaussian Inc., Wallingford, CT, 2009.
- [29] H.B. Schlegel, *J. Comput. Chem.* 3 (1982) 214–218.
- [30] N. Sundaraganesan, S. Ilakiamani, H. Saleem, P.M. Wojciechowski, D. Michalska, *Spectrochim. Acta A* 61 (2005) 2995–3001.
- [31] J. Baker, A.A. Jarzecki, P. Pulay, *J. Phys. Chem. A* 102 (1998) 1412–1424.
- [32] K. Wolinski, J.F. Hinton, P. Pulay, *J. Am. Chem. Soc.* 112 (1990) 8251–8260.
- [33] E. Runge, E.K.U. Gross, *Phys. Rev. Lett.* 52 (1984) 997–1000.
- [34] M. Petersilka, U.J. Gossmann, E.K.U. Gross, *Phys. Rev. Lett.* 76 (1996) 1212–1215.
- [35] R. Bauernschmitt, R. Ahlrichs, *Chem. Phys. Lett.* 256 (1996) 454–464.
- [36] T.W. Hambley, H.K. Chan, I. Gonda, *J. Am. Chem. Soc.* 108 (1986) 2103–2105.
- [37] M. Nethaji, V. Pattabhi, G.R. Desiraju, *Acta Cryst. C* 44 (1988) 275–277.
- [38] S. LoEhr, M. Yonemura, A. Orita, N. Imai, H. Akashi, J. Otera, *Acta Cryst. E59* (2003) 594–595.
- [39] B.G. Johnson, P.M. Gill, J.A. Pople, *J. Chem. Phys.* 98 (1993) 5612–5626.
- [40] D. Sajan, L. Joseph, N. Vijayan, M. Karabacak, *Spectrochim. Acta A* 81 (2011) 85–98.
- [41] L.J. Bellamy, *The Infrared Spectra of Complex Molecules*, vol. 2, Chapman and Hall, London, 1980.
- [42] M. Silverstein, G.C. Basseler, C. Morill, *Spectrometric Identification of Organic Compounds*, Wiley, New York, 1981.
- [43] L.J. Bellamy, R.L. Williams, *Spectrochim. Acta* 9 (1957) 341–345.
- [44] V.K. Rastogi, M.A. Palafox, R.P. Tanwar, L. Mittal, *Spectrochim. Acta A* 58 (2002) 1987–2004.
- [45] G. Varsanyi, *Assignments of Vibrational Spectra of Seven Hundred Benzene Derivatives*, vol. 1, Adam Hilger, 1974.
- [46] D. Sajan, J. Binoy, B. Pradeep, K. Venkatakrishnan, V.B. Kartha, I.H. Joe, V.S. Jayakumar, *Spectrochim. Acta A* 60 (2004) 173–180.
- [47] K. Wolinski, J.F. Hinton, P. Pulay, *J. Am. Chem. Soc.* 112 (1990) 8251–8260.
- [48] D. Lin-Vien, N.B. Colthup, W.G. Fateley, J.G. Grasselli, *The Handbook of Infrared and Raman Characteristic Frequencies of Organic Molecules*, Academic Press, Boston, MA, 1991.
- [49] J. Svoboda, J. Sedlacek, J. Zednik, G. Dvorakova, O. Trhlikova, D. Redrova, *J. Polym. Sci. A Polym. Chem.* 46 (2008) 2776–2787.
- [50] L.J. Bellamy, *Advances in Infrared Group Frequencies*, Methuen London, 1968.
- [51] R. Ditchfield, *Mol. Phys.* 27 (1974) 789–807.
- [52] M. Cossi, V. Barone, B. Mennucci, J. Tomasi, *Chem. Phys. Lett.* 286 (1998) 253–260.
- [53] K. Pihlajer, E. Kleinpeter (Eds.), *Carbon <sup>13</sup>Chemical Shifts Instructure and Spectrochemical Analysis*, VCH Publishers, Deerfield Beach, 1994.
- [54] N. Subramania, N. Sundaraganesan, J. Jayabharathi, *Spectrochim. Acta A* 76 (2010) 259–269.
- [55] H.O. Kalinowski, S. Berger, S. Brawn, *Carbon 13 NMR Spectroscopy*, John Wiley and Sons, Chichester, 1988.
- [56] R. Hoffmann, *Solids and Surfaces: A Chemist's View of Bonding in Extended Structures*, VCH Publishers, New York, 1988.
- [57] J.G. Malecki, *Polyhedron* 29 (2010) 1973–1979.
- [58] N.M. O'Boyle, A.L. Tenderholt, K.M. Langner, *J. Comp. Chem.* 29 (2008) 839–845.
- [59] M. Chen, U.V. Waghmare, C.M. Friend, E. Kaxiras, *J. Chem. Phys.* 109 (1998) 6854–6860.
- [60] K. Fukui, *Science* 218 (1982) 747–754.
- [61] B. Kosar, C. Albayrak, *Spectrochim. Acta A* 78 (2011) 160–167.
- [62] R.G. Pearson, *Proc. Natl. Acad. Sci. USA* 83 (1986) 8440–8841.
- [63] J.S. Murray, K. Sen, *Molecular Electrostatic Potentials, Concepts and 399 Applications*, Elsevier, Amsterdam, 1996.
- [64] E. Scrocco, J. Tomasi, in: P. Lowdin (Ed.), *Advances in Quantum Chemistry*, Academic Press, New York, 1978.